CMS Physics Analysis Summary

Contact: cms-pag-conveners-top@cern.ch 2011/03/14

Search for Resonances in Semi-leptonic Top-pair Decays Close to Production Threshold

The CMS Collaboration

Abstract

We present the results of a search for massive neutral bosons decaying via a top-antitop quark pair. The analysis is based on 36 pb^{-1} of proton-proton collision data at a centre-of-mass energy of 7 TeV collected by the CMS detector at the LHC during 2010. From a combined analysis of the muon plus jets and electron plus jets decay modes no significant signal is observed, and upper limits on the production cross section as a function of the boson mass are reported.

1 Introduction

Numerous extensions to the Standard Model (SM) predict gauge interactions whose couplings with the third-generation quarks, and in particular the top quark, are enhanced [1–8]. These result in new particles, referred to generically as Z′, which could show up as resonances in top-pair production at the LHC and not necessarily in other channels with jets and leptons because of their small couplings to light particles. The associated production of scalar particles, or the supersymmetric production of scalar-top quarks decaying into top-quark pairs and undetected particles, may also result in the distortion of the invariant $\mathrm{t\bar{t}}$ mass distribution without the presence of resonances. Signals of new physics in top-pair production have been searched for by the Tevatron experiments [9–11] which provide the current lower mass limits for a narrow resonance. A narrow topcolor leptophobic $\mathrm{t\bar{t}}$ resonance is excluded for masses below about 800 GeV/c^2.

We present results from the CMS experiment at the LHC based on 36 pb^{-1} of data collected at a center-of-mass energy of 7 TeV during 2010. The analysis focuses on decay channels of the $\mathrm{t\bar{t}}$ system that include a single electron or muon to search for deviations of the $\mathrm{t\bar{t}}$ mass distribution from SM expectations. The event reconstruction and selection is optimised for the production of top quarks close to rest, with well separated decay products. The reference model is a Z′ with narrow width (1% of its mass) so the analysis is applicable to any narrow resonance decaying into $\mathrm{t\bar{t}}$. The analysis sets model-independent limits on the production cross section for such particles as a function of the resonance mass $m_{Z'}$.

2 Analysis Strategy

We search for a Z′ decaying into a $\mathrm{t\bar{t}}$ pair, each top quark decaying into a bottom quark and a W boson, in which one of the W bosons decays hadronically and the other W boson decays into a lepton (a muon or electron) and a neutrino. The experimental signature consists of events containing an energetic isolated lepton in an energetic hadronic environment with two heavy flavour jets. The main backgrounds to this signature are:

- SM $\mathrm{t\bar{t}}$ production
- W boson/Drell-Yan plus jet production, where the jets may contain heavy flavour quarks (W/Z+HF) or only light flavour quarks (W/Z+LF)
- Single top production
- QCD multijet production, including heavy flavour.

QCD multijet background is suppressed by requiring the energetic lepton to be isolated, and the W/Drell-Yan plus jets backgrounds by requiring at least three jets in the event. For each lepton flavour (electron and muon) the data are further divided into four categories according to the total number of jets and the number of jets which have been identified as containing a bottom quark. This differentiation of samples with different signal-to-background ratios improves the overall sensitivity of the analysis. For each category, the mass of the $\mathrm{t\bar{t}}$ pair is estimated. The eight $m_{\mathrm{t\bar{t}}}$ distributions are combined in a joint Bayesian integration.

In the simultaneous integration of the $m_{\mathrm{t\bar{t}}}$ distributions, the background in each is described by a sum of the individual components listed above. The QCD multijet events are estimated from data. All other backgrounds as well as the Z′ signal are modelled using Monte Carlo simulation. The $m_{\mathrm{t\bar{t}}}$ distribution for each of these background types and for each of the eight event categories defines a Probability Density Function (pdf) called a 'template'. Both the normalisations and the shapes of templates can change in the integration. An important aspect of this

analysis is that some of the key systematics are constrained from data, thereby improving the overall background modelling.

The background-only model is built by combining the templates for all backgrounds. The model that includes the Z′ signal is obtained by adding the Z′ template to the SM contribution. The signal-plus-background Likelihood therefore uses the Z′ cross-section as the parameter of interest and the parameters that govern the normalisations and shapes of the background templates are treated as nuisance parameters. Upper limits on the Z′ production are obtained using a Bayesian procedure.

3 The CMS Detector

The central feature of the CMS apparatus is a superconducting solenoid, 13 m in length and 6 m in diameter, which provides an axial magnetic field of 3.8 T. The bore of the solenoid is outfitted with various particle detection systems. Charged particle trajectories are measured by the silicon pixel and strip tracker, covering $0 < \phi < 2\pi$ in azimuth and $|\eta| < 2.5$, where the pseudorapidity η is defined as $\eta = -\ln[\tan\theta/2]$, with θ being the polar angle of the trajectory of the particle with respect to the beam direction. A crystal electromagnetic calorimeter (ECAL) and a brass/scintillator hadronic calorimeter surround the tracking volume. In this analysis the calorimetry provides high-resolution energy and direction measurements of electrons and hadronic jets. Muons are measured in gas detectors embedded in the steel return yoke outside the solenoid. The detector is nearly hermetic, allowing for energy balance measurements in the plane transverse to the beam directions. A two-tier trigger system selects the most interesting pp collision events for use in physics analysis. A more detailed description of the CMS detector can be found elsewhere [12].

4 Signal and Background Modelling

Signal and background processes are simulated by MADEVENT/MADGRAPH [13], PYTHIA6 [14] and MC@NLO [15] event generators using CTEQ6L parton distribution functions [16]. PYTHIA6 is used to describe the radiation and fragmentation using the prescriptions in [17] and implements a CMS custom underlying event tuning [18]. All Monte Carlo events were fully simulated and reconstructed via the CMS simulation and reconstruction software.

W boson and Drell-Yan production in association with up to four jets is generated with MADGRAPH, with additional jet production described via matrix elements which are matched to parton showers via the MLM prescription [19] with a matching threshold of 20 GeV. The inclusive next-to-next-to-leading order cross sections are used [20]: 31.3 nb for W with subsequent decays into leptons, and 3.05 nb for Drell-Yan production of dilepton final states with invariant mass $> 50\,\mathrm{GeV}/c^2$. QCD multi-jet processes are simulated using PYTHIA6.

SM top-quark pair events are generated with MADGRAPH, including spin correlation in the top decays. Higher order gluon and quark production is described via matrix elements, with up to three extra partons beyond the top-quark pair system. The chosen threshold for the parton shower to matrix element matching is 30 GeV. An additional $\mathrm{t\bar{t}}$ sample is generated using MC@NLO to provide a cross check and allow an estimate of systematic uncertainties in the modelling. For the top-quark pair production, the inclusive cross section value of 157.5 pb is used [21, 22].

Single top production is also modelled in MADGRAPH. The t-channel single top next-to-leading order cross section, multiplied by the leptonic branching fraction $BR(\mathrm{W} \to l\nu)$, has

been determined as 21.0 pb using MCFM [21, 23–25]. For single top quark associated production (tW), a value of $\sigma \times BR(\mathrm{W} \to l\nu) = 10.6$ pb [24] is used.

As a reference model for new physics, MADGRAPH is also used to generate Z′ bosons decaying to $\mathrm{t\bar{t}}$ pairs with a range of masses between 500 GeV/c^2 and 2 TeV/c^2. The width of the resonance is set to 1% of its mass so as to be narrower than the experimental resolution.

5 Event Selection

We search for Z′ using the electron plus jets and muon plus jets signatures. Events in the data sample were selected using either a single muon or single electron trigger. The initial muon trigger requirement was for a muon candidate with momentum transverse to the beam direction $p_{\mathrm{T}} > 9$ GeV/c. The threshold was later raised to 15 GeV/c to maintain acceptable rates as the luminosity increased. The electron trigger threshold applied to the transverse energy of a cluster of measurements in the ECAL also increased during the 2010 run, from $E_{\mathrm{T}} = 10\,\mathrm{GeV}$ to $E_{\mathrm{T}} = 22\,\mathrm{GeV}$.

Muons are reconstructed using the information from the muon chambers and the silicon tracker [26]. Tracks are required to have at least 11 hits in the tracker and at least one in the pixel layers, and the global track fit must have normalised $\chi^2 < 10$. The tracks must also pass within 0.02 cm of the primary vertex in the plane transverse to the beam, and within 1 cm along the beam axis. Muon candidates are additionally required to have $p_{\mathrm{T}} > 20$ GeV/c and $|\eta| < 2.1$.

Electrons are identified using a combination of the shower-shape information and the quality of the match between the track and electromagnetic cluster [27]. Electron candidates are required to have $p_{\mathrm{T}} > 30$ GeV/c and $|\eta| < 2.5$, excluding the transition region between the barrel and forward calorimeters, $1.4442 < |\eta| < 1.566$. Electrons coming from photon conversions in the detector material are rejected by requiring that the electron track has an associated hit in the innermost pixel layer. Additionally since photon conversions typically produce two tracks with very small angular separation, it is required that there is no other track with a similar polar angle ($\Delta \arctan(\theta) < 0.02$) within 0.02 cm in the transverse plane (measured where the tracks are parallel).

To select leptonic W boson decays, events are required to contain either one isolated muon or one isolated electron. The isolation requirement is based on the ratio of the total transverse energy observed from all hadrons and photons in a cone of size $\Delta R = \sqrt{\Delta\phi^2 + \Delta\eta^2} < 0.3$ around the lepton direction to the transverse momentum of the lepton itself, known as relative isolation. This quantity must be less than 10%.

In order to reduce the background from Drell-Yan production and $\mathrm{t\bar{t}}$ production in which both W bosons decay leptonically, events in which two lepton candidates are identified are vetoed. To increase the rejection, the second lepton may be allowed to satisfy looser requirements: an additional muon must have $p_{\mathrm{T}} > 10$ GeV/c, $|\eta| < 2.5$ and relative isolation < 0.2; an electron in an event with a muon candidate must have $p_{\mathrm{T}} > 15$ GeV/c, $|\eta| < 2.5$ and relative isolation < 0.2; and electrons which form an invariant mass close to that of the Z boson when combined with the first electron candidate (between 76 GeV/c^2 and 106 GeV/c^2) are required to have $p_{\mathrm{T}} > 30$ GeV/c, $|\eta| < 2.5$ and relative isolation < 1.0.

Events are additionally required to contain at least three jets, reconstructed using an anti-Kt clustering algorithm with a cone parameter $\Delta R = 0.5$ [28]. The jet energies are calculated using a particle flow algorithm [29] and both relative and absolute jet energy corrections are applied to account for the dependence of the jet response as a function of η and p_{T}, respectively [30].

Jet candidates are required to have $p_T > 30$ GeV/c and $|\eta| < 2.4$, and must not overlap with any lepton candidate within $\Delta R < 0.4$. To enhance the rejection of background from W boson and Drell-Yan production in association with relatively low p_T jets, the leading jet is required to have $p_T > 70$ GeV/c and the second leading jet to have $p_T > 50$ GeV/c.

The negative of the vector sum of the momenta of all reconstructed jets and leptons in the plane transverse to the beam is the missing transverse energy E_T^{miss} vector [31]. QCD background is suppressed further by requiring $E_T^{miss} > 20$ GeV.

6 Reconstruction

For each lepton flavour, events are separated into four categories according to the total number of jets and the number of jets which have been identified as candidates to originate from bottom quarks ("b tagged") by the reconstruction of a displaced vertex [32]. The displaced vertex algorithm is tuned to give a mistag rate on 100 GeV light-quark jets of approximately 2%, with a corresponding efficiency of tagging b jets in $t\bar{t}$ decays of around 60% in the central region. The categories are: events with three jets of which at least one is b tagged; events with four or more jets and no b-tagged jet; events with four or more jets and exactly one b-tagged jet; and events with four or more jets of which at least two are b tagged.

The reconstruction of $m_{t\bar{t}}$ is done in three steps: first a leptonically decaying W boson is reconstructed; then the jets are associated to partons in the $t\bar{t}$ decay chain; and finally a kinematic fit is performed.

It is assumed that one W boson from a top decay has decayed into the observed lepton and an undetected neutrino. The E_T^{miss} is taken as a measurement of the transverse momentum of the neutrino, but its longitudinal momentum (i.e. parallel to the beam direction) is unmeasured. Imposing the condition that the invariant mass of the lepton and neutrino is the mass of the W boson (80.4 GeV/c^2) allows the construction of a quadratic equation for the longitudinal momentum of the neutrino. If there are two real solutions, both are retained. If the equation only has imaginary solutions, the components of E_T^{miss} are modified by the minimal amount in $|\Delta {E_T^{miss}}_x| + |\Delta {E_T^{miss}}_y|$ to give one real solution.

The association of the jets to the hadronic W decay and to the two b quarks is done by calculating a χ^2 for each possible combination (including the two neutrino solutions if they are both physical and only allowing b tagged jets to be associated to a bottom quark) and choosing the combination with the smallest value. The χ^2 is a sum over several terms

$$\chi^2 = \sum \chi_i^2 = \sum \frac{(x_i - x_{i\,ref})^2}{\sigma_i^2}$$

where x_i is a reconstructed quantity, $x_{i\,ref}$ is a reference value for this quantity and σ_i is a resolution parameter. The reconstructed quantities and the central values and widths used are listed in Table 1. The appropriate reference values and resolutions for the masses are obtained from the distributions of these quantities in the Monte Carlo simulation. Since no flavour-specific jet energy scale corrections are applied, deviations from the generated values of the top quark and W boson masses are expected. The association of jets to the W boson and the bottom quarks is found to be correct in approximately 80% of events in the simulation.

To optimise the measurement of $m_{t\bar{t}}$ a kinematic fit is performed in which the four-momenta of the reconstructed objects are varied within their known resolutions. Mass constraints of 172.5 and 80.4 GeV/c^2 are used for the top quarks and the W bosons respectively. The improvement in resolution can be seen in Figure 1.

Quantity	Reference Value	Resolution
Leptonic Top Mass	169.0 GeV/c^2	16.3 GeV/c^2
Hadronic Top Mass	174.7 GeV/c^2	14.6 GeV/c^2
Hadronic W Mass	83 GeV/c^2	10.9 GeV/c^2
p_T of $t\bar{t}$ System	0 GeV/c	50 GeV/c
H_T Fraction	1.	0.15

Table 1: Quantities, with their reference values and resolutions, used in the definition of the χ^2 for jet-parton association. The 'H_T Fraction' is the scalar sum of the transverse energy in the selected jets divided by the scalar sum of the transverse energy in all jets.

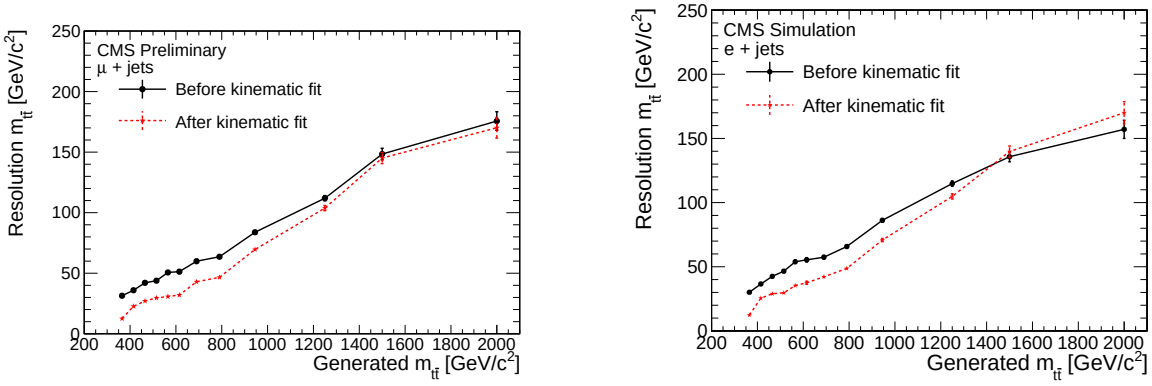

Figure 1: Resolution of reconstructed $m_{t\bar{t}}$ as a function of generated $m_{t\bar{t}}$ for muon plus jets events (left) and electron plus jets events (right).

7 Background Estimation

We divide the SM backgrounds into three categories and, where possible, use the data to constrain both the rates and kinematic shapes of each. These contributions are QCD multijet events, W boson/Drell-Yan plus jets events and $t\bar{t}$ events. We also account for the small contribution from single top quark production.

7.1 QCD Multijet Events

QCD multijet events can be mis-reconstructed as a lepton plus jets signature, even though this is highly suppressed by the isolation requirement. Although semileptonic and leptonic decays of hadrons contribute to both channels, energetic photon conversions will only contaminate the electron channel. The contribution of this background to muon plus jets and electron plus jets samples is therefore determined separately.

The yields in the muon sample are determined with a matrix method [33]. A loose region which is a superset of the tight region containing the signal is first defined, in this case by relaxing the cut on the relative isolation from 10% to 100%. The number of QCD events in the signal region can then be calculated from: the total number of events in the loose region; the fraction of muons from QCD events in the loose region that are also in the tight region; and the fraction of muons from non-QCD events in the loose region that are also in the tight region. The fraction of muons from QCD events falling in the tight region is calculated from a control region; the fraction in non-QCD events is taken from simulation and verified using the tag-and-probe method.

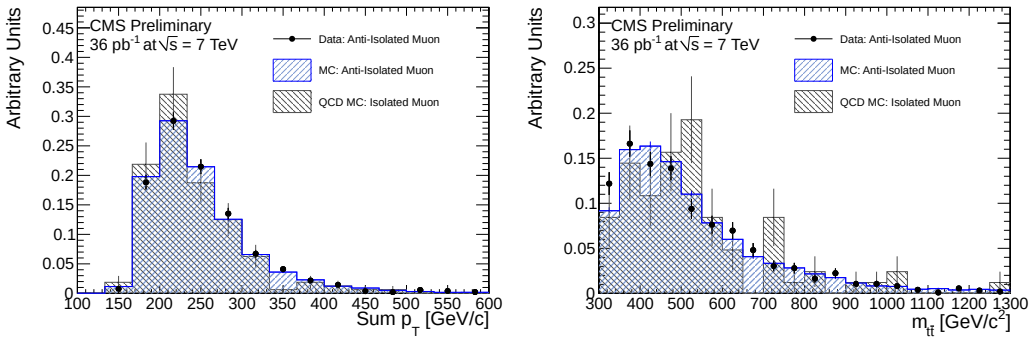

Figure 2: Comparison of the QCD background shapes in the muon channel, showing the distribution of the scalar sum of p_{T} in events with exactly two jets (left) and the distribution of $m_{\mathrm{t\bar{t}}}$ in events with exactly three jets (right).

Systematic uncertainties on the predicted yields are estimated by varying the definitions of the loose isolation cut and of the control region, and by changing the efficiency for prompt muons within uncertainties. Variations of up to 70% are observed. The muon channel results, shown in Table 2, indicate that the simulation underestimates the background by roughly a factor of two in the three-jet and more in the four-jet events. Cross-checks performed using other two-variable spaces lead to the same conclusions.

N_{Jets}, N_{B-tags}	3, ≥ 0	3, ≥ 1	4, ≥ 0	4, ≥ 1
$N_{true,MC}$	10.6 ± 1.1	2.6 ± 0.5	2.3 ± 0.5	0.6 ± 0.3
$N_{MC,obs}$	14.0 ± 8.8	4.2 ± 4.0	3.7 ± 3.6	1.5 ± 1.8
$N_{Data,obs}$	22.5 ± 11.3	8.2 ± 7.2	10.8 ± 8.8	6.2 ± 4.7

Table 2: Estimated number of QCD background events in the muon channel for events with 3 and 4 jets and 0 and 1 b-tags. In the first row $N_{true,MC}$ is the normalised actual number of QCD background events in the simulated sample and the error is purely statistical. In the second row $N_{MC,obs}$ is the number of background events in simulation extracted by the method described and in the third row $N_{Data,obs}$ is the number of background events extracted in the data. The latter two rows include both systematic and statistical uncertainties. Note that the b tag categories are inclusive.

As the QCD isolated muon background is expected to be predominantly from hadronic decays, the shape of the muon QCD background is determined from an independent set of events selected by inverting the isolation cut on the muons and raising the threshold slightly to ensure minimal contamination from non-QCD events. The distribution of the background is found to be in good agreement with that in simulated isolated muon events (Figure 2). The final QCD model for the muon channel uses this shape normalised to the yield estimated from the matrix method.

The number of QCD background events in the electron sample is evaluated by removing the isolation cut in data, fitting the distribution of relative isolation in this sample to a simple function (e.g. a gaussian tail) in a region with high relative isolation, and then extrapolating the fit into the region with relative isolation $< 10\%$ that is selected for the analysis. As the fit is sensitive to the exact boundaries selected, both the fit range and the form of the fit function are varied and the average of the results is taken as the best estimate. An uncertainty of 70% is representative of the observed variation.

The QCD background in the electron channel is expected to consist of both hadronic decays and

photon conversions, of which the latter dominates. The shape is therefore determined from a control sample formed by inverting the veto on photon conversions described in Section 5. This provides an almost pure sample of QCD events, and the bias in the shape from choosing a conversion-rich QCD sample is small compared to the statistical error. The final QCD model for the electron channel uses the shape taken from this control sample with the yields from the isolation energy fits.

To account for all of the calculated errors and the uncertainty of extrapolating into low-statistics regions, a total systematic error of 100% is applied to the QCD background in both the electron and muon channels.

7.2 Other Backgrounds

The shape and rate of the contributions to the $m_{t\bar{t}}$ distribution from W and Drell-Yan plus jets, $t\bar{t}$ and single top production are obtained from simulation using theoretical cross-sections. Diboson production contributes a negligible amount and is ignored.

The summary of the yields of all eight categories of background events that contribute to the signal region is given in Table 3.

Yields	$t\bar{t}$	W/Z+LF	W/Z+HF	Single-top	QCD	Data	Sum BG
μ 3j1t	96.9 ± 0.6	7.9 ± 0.2	28.6 ± 1.1	11.6 ± 0.1	8.2 ± 8.2	142 ± 11.9	153.2 ± 8.3
μ 4j0t	40.4 ± 0.5	62.8 ± 2.2	25.0 ± 1.0	2.5 ± 0.1	4.5 ± 4.5	107 ± 10.3	135.1 ± 5.1
μ 4j1t	84.8 ± 0.6	3.8 ± 0.1	12.5 ± 0.7	4.2 ± 0.1	5.1 ± 5.1	112 ± 10.6	110.5 ± 5.2
μ 4j2t	51.6 ± 0.4	0.1 ± 0.0	2.4 ± 0.2	2.0 ± 0.0	1.0 ± 1.0	58 ± 7.6	57.1 ± 1.1
e 3j1t	80.3 ± 0.6	5.4 ± 0.1	22.8 ± 1.0	8.5 ± 0.1	9.4 ± 9.4	114 ± 10.7	126.4 ± 9.5
e 4j0t	31.8 ± 0.4	47.0 ± 1.9	19.1 ± 0.9	1.9 ± 0.0	10.8 ± 10.8	106 ± 10.3	110.4 ± 11.0
e 4j1t	66.7 ± 0.5	2.8 ± 0.1	9.0 ± 0.6	3.2 ± 0.1	3.0 ± 3.0	80 ± 8.9	84.7 ± 3.1
e 4j2t	40.9 ± 0.4	0.1 ± 0.0	2.1 ± 0.2	1.5 ± 0.0	0.1 ± 0.1	50 ± 7.1	44.6 ± 0.5

Table 3: Expected and observed event yields in the eight categories defining the signal region used for the statistical evaluation for 36 pb^{-1}. All expected yields are taken from simulation except for the QCD contributions which are taken from the data-driven methods. The uncertainties in the first four columns and the data are purely statistical, while those for QCD are combined systematic and statistical and are taken conservatively to be 100%. Note that the categories are exclusive.

8 Systematic Uncertainties

The trigger, lepton identification and isolation efficiencies are evaluated using simulation and verified using data. For these a standard tag-and-probe analysis [34] is performed using $Z^0 \rightarrow ll$ events extracted from data. The efficiencies are found to have the same dependency on the lepton p_T and η in data and simulation and a constant scale factor is applied.

The systematic effects due to the uncertainties in the cross sections used in the simulations of the $t\bar{t}$, single top and W/Drell-Yan backgrounds are obtained by varying each one in turn within its uncertainty, and repeating the event selection and reconstruction to produce modified $m_{t\bar{t}}$ distributions. The same procedure is used to propagate the errors on the QCD background estimates, energy scales and resolutions and heavy flavour tagging efficiencies. Additional uncertainties in the modelling of events is accounted for by varying the renormalisation

and factorisation (Q^2) scale for $t\bar{t}$ and W/Drell-Yan production, the matching scale for $t\bar{t}$ production and the amount of initial and final state radiation in $t\bar{t}$ production within a suitable range. A further uncertainty is associated with the difference between $t\bar{t}$ production models.

Uncertainty	Variation	Type
Luminosity	4%	rate
Electron efficiency (trigger + ID + isolation)	5%	rate
Muon efficiency (trigger + ID + isolation)	5%	rate
$t\bar{t}$ cross section	20%	rate
Single top cross section	30%	rate
W+jets cross section	50%	rate
Ratio Drell-Yan to W cross section	30%	rate
Ratio W/Z+HF to σ(W)	100%	rate
Muon QCD yield	100%	rate
Electron QCD yield	100%	rate
Jet energy scale	p_T,η dependent	shape
Jet energy resolution	10%	shape
Unclustered energy	10%	shape
b tagging efficiency (b jets)	15%	shape
b tagging efficiency (c jets)	30%	shape
Q^2 scale for W and Drell-Yan events	$\pm 1\sigma$ generator parameters	shape
$t\bar{t}$ modelling	$\pm 1\sigma$ generator differences	shape
Q^2 scale for $t\bar{t}$ events	$\pm 1\sigma$ generator parameters	shape
Amount of ISR/FSR for $t\bar{t}$ events	$\pm 1\sigma$ generator parameters	shape
Matching scale for $t\bar{t}$ events	$\pm 1\sigma$ generator parameters	shape

Table 4: Summary of relative systematic uncertainties and whether they are rate- or shape-changing.

Table 4 summarises the systematic uncertainties and the relative variations of the individual quantities. Theoretical uncertainties on the $t\bar{t}$ and W+jets modelling are calculated from dedicated samples which correspond to changes of two parameters in the MC generation: the threshold for the jet matching between the matrix element and the parton shower generators, and the renormalisation and factorisation scale. Both parameters are varied by a factor of 0.5–2. Rate-changing uncertainties affect the rate of single or several samples; shape-changing uncertainties influence both the rates and shapes of the $m_{t\bar{t}}$ distributions.

The jet energy scale uncertainties are less than 3% and come from p_T- and η-dependent uncertainties which were derived in jet events in the first $3\,\mathrm{pb}^{-1}$ of data. For this reason, an uncertainty of 1.5% is added in quadrature to account for calibration changes. Additional p_T-dependent uncertainties due to pile-up as well as supplementary uncertainties for b-flavoured jets are typically at the 2-3% level and are added in quadrature.

9 Statistical Description

We model the eight binned $m_{t\bar{t}}$ distributions by combining the templates for the signal and all backgrounds. The total number of predicted events for the bin corresponding to $t\bar{t}$ invariant

mass $m_{t\bar{t}}$, $n_k(m_{t\bar{t}})$, in the k-th event category (one of eight) is:

$$\begin{aligned} n_k(m_{t\bar{t}}, \vec{\sigma}^r, \vec{\sigma}^s) &= N_k^{signal}(\vec{\sigma}^r, \vec{\sigma}^s) \cdot \text{pdf}^{signal}(m_{t\bar{t}}, \vec{\sigma}^s) \\ &+ \sum_i N_{ki}^{background}(\vec{\sigma}^r, \vec{\sigma}^s) \cdot \text{pdf}^{background}(m_{t\bar{t}}, \vec{\sigma}^s), \end{aligned} \quad (1)$$

where i is the background type (SM $t\bar{t}$, W+jets, QCD, etc.). The signal normalisation $N_k^{signal}(\vec{\sigma}^r, \vec{\sigma}^s)$ and the background normalisations $N_{ki}^{background}(\vec{\sigma}^r, \vec{\sigma}^s)$ depend on the rate-changing parameters, $\vec{\sigma}^r$, and on the shape-changing parameters, $\vec{\sigma}^s$. The templates themselves ($\text{pdf}(m_{t\bar{t}}, \vec{\sigma}^s)$) depend only on the latter. The most important rate-changing parameters are the cross-sections themselves. Technically, we implement them as multiplicative scale factors with respect to the theoretical predictions. The parameter of interest is the Z′ cross section. All others are nuisance parameters and describe the impact of the systematic uncertainties on the measurement.

As we employ a Bayesian approach, we assign priors to all nuisance parameters. The rate-changing uncertainties with a relative size smaller than 30% are assigned Gaussian priors; otherwise, log-normal priors are used. For shape-changing uncertainties, a bin-wise interpolation between histogram templates at different variations of the respective uncertainty is used (template morphing). These are derived by changing each uncertainty by ± 1 standard deviation with respect to the nominal values. The interpolation is performed in each bin using a cubic function, continuing smoothly with linear functions beyond $\pm 1\sigma$. The associated nuisance parameters have a Gaussian prior with mean 0 and width 1 and are correlated among all affected bins and samples.

To set limits on the production cross-section of an additional Z′ boson, a Markov chain Monte Carlo is used to perform a full Bayesian numerical integration.

9.1 Comparison of the Data and the Standard Model

Figures 3 and 4 show the data in the muon and electron channels respectively, as a function of $m_{t\bar{t}}$. The four plots correspond to the different categories of data events as defined in Section 6. The solid histograms are the sum of the SM processes normalised to the medians of the posterior distributions obtained by Bayesian integration of the Likelihood over the priors.

Also shown as open histograms are the expectations for Z′ production with masses of 500 GeV/c^2, 750 GeV/c^2, 1000 GeV/c^2, and 1250 GeV/c^2, scaled to a cross section of 50 pb. We find good agreement between the data and expected SM event yields in both channels and for each event category.

9.2 Limit Setting for Z′ Production

Having established good agreement with the SM, we proceed to set limits on the Z′ production cross section. For this parameter, we assume a flat prior. To support this choice, we perform coverage tests by generating pseudo-experiments, taking all uncertainties into account, with fixed Z′ cross sections for two Z′ models. A full Bayesian integration is carried out in each pseudo-experiment, and the 95% confidence level upper limits are calculated from the 95% quantile of the posterior probability density of the signal cross section. As no more than 5% of these upper limits are below the input cross section, the method has coverage. Expected upper limits on the Z′ production cross section are calculated using background-only pseudo-experiments. The median of the distribution of upper limits defines the expected upper limit, and the central 68% and 95% of the distribution give the central 68% and 95% bands of expected upper limits.

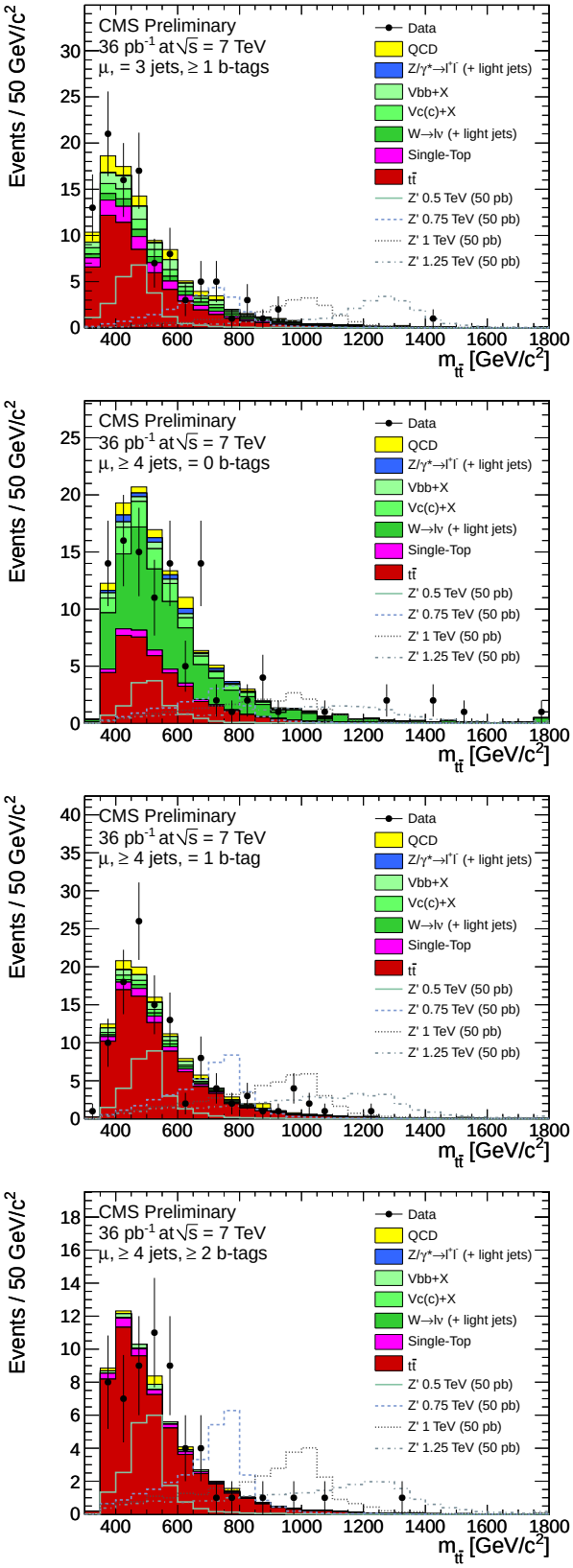

Figure 3: Reconstructed $m_{\mathrm{t\bar{t}}}$ using leading 3 jets (3-jet events with at least one b tag) and reconstructed $m_{\mathrm{t\bar{t}}}$ after kinematic fit (4-jet events with 0, 1, and at least two b tags) in the muon + jets channel.

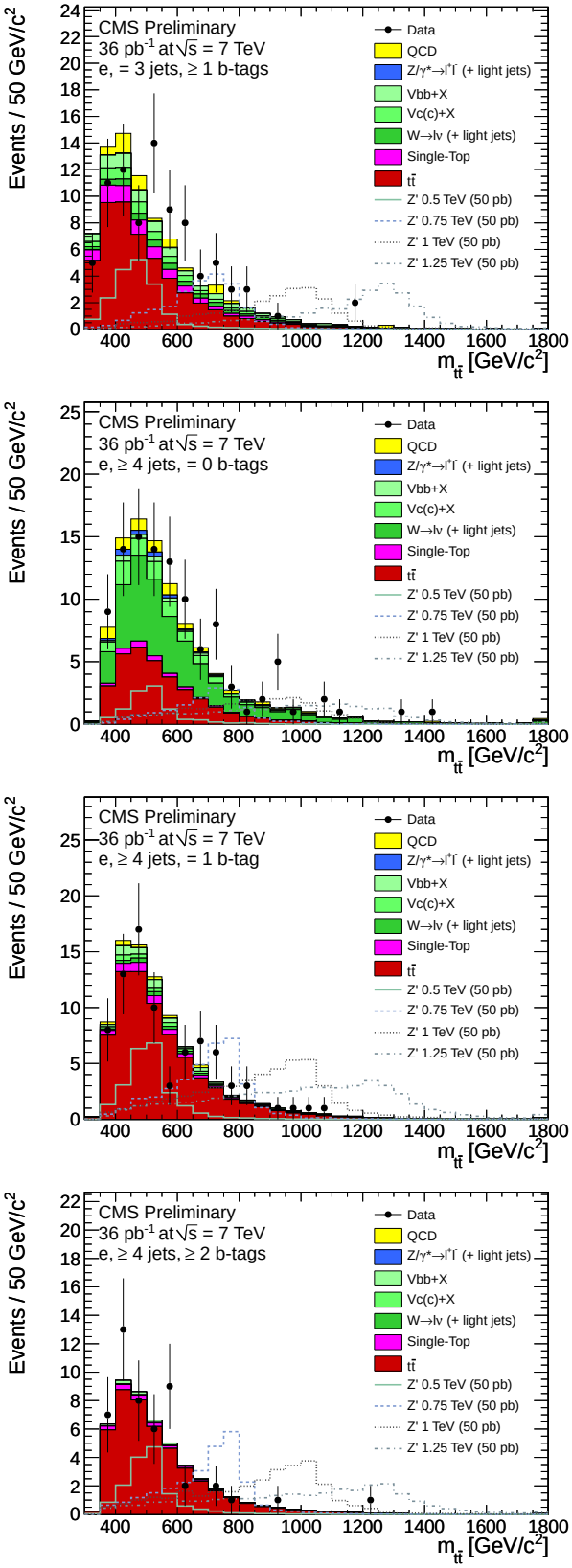

Figure 4: Reconstructed $m_{\mathrm{t\bar{t}}}$ using leading 3 jets (3-jet events with at least one b tag) and reconstructed $m_{\mathrm{t\bar{t}}}$ after kinematic fit (4-jet events with 0, 1, and at least 2 b tags) in the electron + jets channel.

10 Results

A simultaneous statistical evaluation of all categories is performed. Expected and observed limits are shown in Figure 5. The observed limits range from approximately 25 pb at a Z' mass of 500 GeV/c^2 to approximately 7 pb at 1 TeV/c^2 and approximately 4 pb at 1.5 TeV/c^2. The observed limits are compatible with the expected limits over the whole mass range, showing a good agreement between simulation and data.

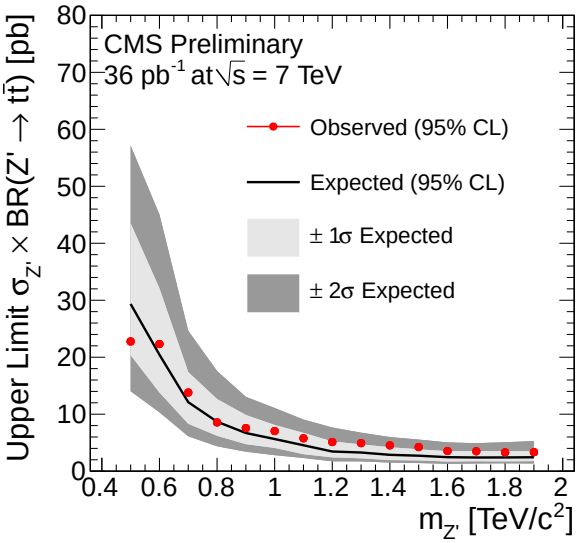

Figure 5: Expected and observed limits from Bayesian integration using Markov chain Monte Carlo for $\sigma(\mathrm{pp} \to Z') \times BR(Z' \to \mathrm{t\bar{t}}\,)$ for $\mathcal{L} = 36\ \mathrm{pb}^{-1}$ as a function of Z' mass. The light grey band indicates the $\pm 1\sigma$ band of the expected limits, and the dark grey band the $\pm 2\sigma$ band of expected limits.

10.1 Cross Check

In order to confirm the basic features of this analysis, an independent analysis has also been performed as a cross-check. This cross-check analysis uses a different selection, background estimation and statistical treatment, and is documented in Appendix A. In particular, the background shape is estimated directly from data, by inverting the b-tagging selection. The cross-check analysis is found to be consistent with the result described above, and again no excess above the SM expectation is seen.

11 Conclusions

This analysis searches for resonances decaying to top quark pairs in the lepton plus jets decay channel. No significant excess of events above SM expectations is seen, and 95% C.L. limits are set on the production of such a resonance assuming that its width is negligible compared to the detector resolution. Limits of the order of 25 pb for invariant masses in the region of $m_{Z'} = 0.5$ TeV/c^2, 7 pb for $m_{Z'} = 1$ TeV/c^2 and 4 pb for $m_{Z'} > 1.5$ TeV/c^2 are set, consistent with those expected. These limits are competitive with those from the Tevatron, particularly at higher masses.

A Cross Check Analysis

A second, independent analysis is also performed as a cross check. The crucial feature of the main analysis is the modelling of each of the background components separately, and in many cases from templates obtained from the Monte Carlo simulation. Therefore, the cross-check analysis uses an entirely data-driven background estimation to reduce systematics from modelling. It also uses different lepton isolation criteria that are less sensitive to the boost of the top quark and hence the $t\bar{t}$ invariant mass, although less effective at rejecting background. Finally, a different algorithm is used for b tagging.

A.1 Selection and Reconstruction

Electron and muon reconstruction is the same as in the main analysis, but the lepton isolation requirement uses a two-dimensional cut in the ΔR_{min} versus $p_{\text{T}}^{\text{rel}}$ plane, where ΔR_{min} is the minimum separation between the lepton and the closest jet of at least 20 GeV/c and $p_{\text{T}}^{\text{rel}}$ is the transverse momentum of the lepton with respect to the jet axis. The thresholds chosen for the analysis are $p_{\text{T}}^{\text{rel}} > 25$ GeV/c and $\Delta R_{\text{min}} > 0.5$ both for muons and electrons. This technique is expected to be less sensitive to the mass of the $t\bar{t}$ system, and will subsequently be referred to as the 2Dcut method.

In order to ensure a high purity sample, four jets are required of which two must have a high probability of being produced by b quarks. This is achieved by requiring that at least two good tracks in the jet have a signed impact parameter significance greater than 1.7, corresponding to a 10% expected rate of "fakes" from light quark jets.

To further increase the sample purity, residual Z plus jets events and $t\bar{t}$ events in which both W bosons have decayed into a lepton are rejected by requiring that there be only one lepton that passes the 2Dcut and no further isolated lepton candidates with $p_{\text{T}} > 10\,\text{GeV}/c$.

Figure 6 shows the final $m_{t\bar{t}}$ distributions from CMS data in the semileptonic muon and electron channels respectively, with a total integrated luminosity of 36 pb^{-1}. The data points are superimposed on the expectation from the SM, divided into the different background contributions.

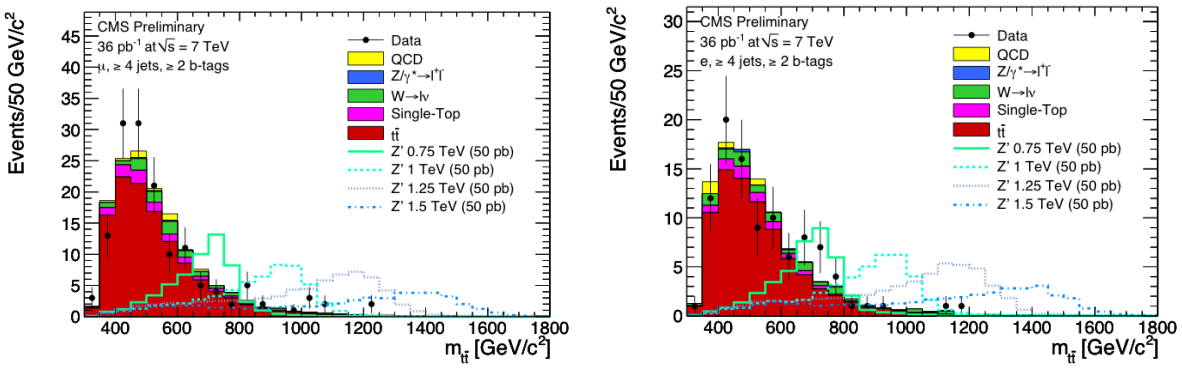

Figure 6: Reconstructed $m_{t\bar{t}}$ in data for 36 pb^{-1} of luminosity, for the muon (left) and electron (right) channels. The data are compared with the expectations of the SM, divided into the various components.

A.2 Limit Setting for Z′ Production

To extract the number of signal events an extended unbinned maximum likelihood fit to the $m_{t\bar{t}}$ distribution is performed. The likelihood fit uses probability density functions derived sep-

arately for the muon and electron channels. The background density functions are taken to be exponentials fitted to control regions defined by requiring that no jets are b tagged. The signal density functions are analytical functions fitted to simulated samples at different Z′ masses.

The semi-muonic and semi-electronic channels are fitted simultaneously, imposing the condition that a hypothetical signal is consistent with the same Z′ in both channels. In the fit, the number of background events and the Z′ cross section are left free to vary. The 95% C.L. upper limits on $\sigma(\mathrm{pp} \to \mathrm{Z}') \times BR(\mathrm{Z}' \to \mathrm{t\bar{t}})$ is obtained by integrating the likelihood of the fit with a prior that the cross section can only be positive.

Monte Carlo pseudo-experiments are used to evaluate the fit performance and reliability, and to determine the expected upper limits on the cross section.

A.3 Systematic uncertainties

Various sources of systematic uncertainty are considered in this analysis, including limited simulation statistics, inadequacies of the modelling in the simulation, and limited knowledge of detector and accelerator properties. For each source of systematic uncertainty, we consider variations of the relevant parameters by $\pm\sigma$, σ being the uncertainty on the parameter that is varied. If the resulting variation of the cross section is asymmetric, the larger effect is taken. Table 5 summarises the systematic uncertainties on the cross-section measurement. We consider the luminosity, b-tagging efficiency and jet energy scale to be fully correlated between the electron and muon channels. All other uncertainties are added in quadrature.

Source	$Z'(750)$	$Z'(1000)$	$Z'(1250)$	$Z'(1500)$
MC statistics (semi-mu) (%)	2.7	4.5	2.2	5.4
MC statistics (semi-e) (%)	3.0	2.8	2.4	3.5
Trigger efficiency (μ) (%)		1.2		
Trigger efficiency (e) (%)		1.9		
b-tagging efficiency (%)		30		
Luminosity (%)		11		
Jet-energy scale (pb)	1.2	3.8	2.4	3.9
Signal peak position (pb)	0.3	0.2	0.0	0.3
Signal peak resolution (pb)	0.4	0.2	0.0	0.2
Signal peak tail (pb)	0.2	0.8	0.1	0.3
Background shape (μ) (pb)	0.5	1.3	0.9	2.1
Background shape (e) (pb)	0.4	0.3	0.3	0.4
Alternative background parameterisation (pb)	0.6	1.6	0.1	0.2
Alternative signal parameterisation (pb)	0.8	1.3	0.2	1.8

Table 5: Systematic uncertainties on the cross section measurement in the cross check analysis.

B Combined Mass Plots

The $m_{\mathrm{t\bar{t}}}$ distribution for all events selected in the main analysis with three jets in both muon and electron channels is shown in Figure 7. Similarly, the $m_{\mathrm{t\bar{t}}}$ distribution for all events selected in the main analysis with four jets is shown in Figure 8. These plots are shown for illustration only, as the inputs to the statistical analysis are the separate categories shown in Figure 3 and Figure 4.

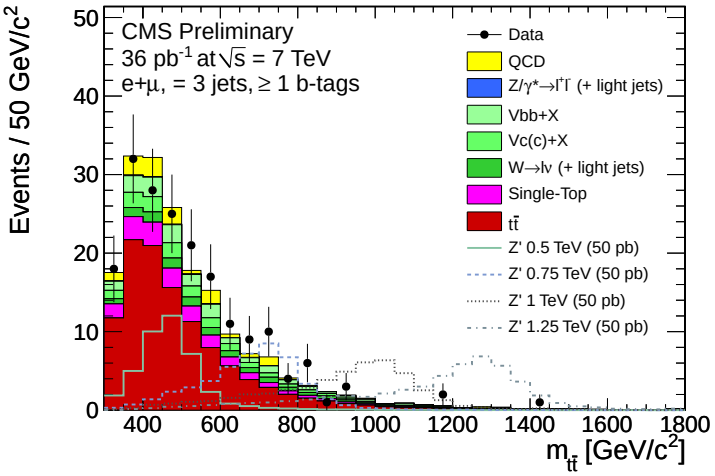

Figure 7: Reconstructed $m_{t\bar{t}}$ using leading 3 jets in 3-jet events with at least one b tag in electron and muon channels combined. *(For illustration only.)*

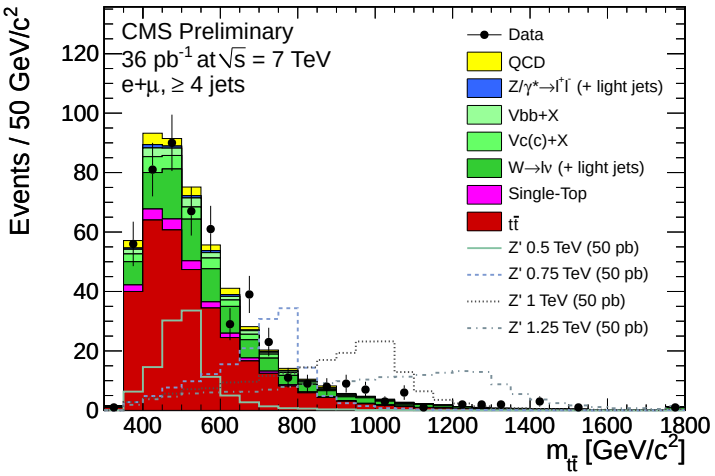

Figure 8: Reconstructed $m_{t\bar{t}}$ in all 4 or more-jet events in electron and muon channels combined. *(For illustration only.)*

References

[1] S. Dimopoulos and H. Georgi *Nucl. Phys.* **B193** 150.

[2] S. Weinberg *Phys. Rev.* **D13** 974.

[3] L. Susskind *Phys. Rev.* **D20** 2619.

[4] C. T. Hill and J. Parke *Phys. Rev.* **D49** 4454.

[5] R. S. Chivukula et al. *Phys. Rev.* **D59** 075003.

[6] N. Arkani-Hamed, A. G. Cohen, and H. Georgi *Phys. Lett.* **B513** 232.

[7] N. Arkani-Hamed, S. Dimopoulos, and G. R. Dvali *Phys. Lett.* **B429** 263.

[8] L. Randall and R. Sundrum *Phys. Rev. Lett.* **83** 3370.

[9] CDF Collaboration *Phys. Rev.* **D 77** 051102.

[10] CDF Collaboration *Phys. Rev. Lett.* **100** 231801.

[11] D0 Collaboration *D0 Note* **5882-CONF**.

[12] CMS Collaboration, "The CMS detector at CERN LHC", *JINST* **0803** (2008).

[13] F. Maltoni and T. Stelzer *hep-ph/0208156*.

[14] T. Sjostrand et al. *Comput. Phys. Commun.* **135** 238.

[15] S. Frixione and B. R. Webber, "The MC@NLO event generator", arXiv:hep-ph/0207182.

[16] D. R. Stump *Proceedings to Amsterdam 2002, ICHEP* 265.

[17] P. Bartalini, R. Chierici, and A. De Roeck *CERN-CMS-NOTE* **2005-013**.

[18] R. Field, "Early LHC Underlying Event Data - Findings and Surprises", arXiv:1010.3558.

[19] S. Hoche et al. *hep-ph/0602031*.

[20] K. Melnikov and F. Petriello, "Electroweak gauge boson production at hadron colliders through O(alpha(s)**2)", *Phys. Rev.* **D74** (2006) 114017, arXiv:hep-ph/0609070. doi:10.1103/PhysRevD.74.114017.

[21] . http://mcfm.fnal.gov/.

[22] R. Kleiss and W. J. Stirling, "Top quark production at hadron colliders: Some useful formulae", *Z. Phys.* **C40** (1988) 419–423. doi:10.1007/BF01548856.

[23] J. M. Campbell, R. Frederix, F. Maltoni et al., "Next-to-Leading-Order Predictions for t-Channel Single-Top Production at Hadron Colliders", *Phys. Rev. Lett.* **102** (2009) 182003, arXiv:0903.0005. doi:10.1103/PhysRevLett.102.182003.

[24] J. M. Campbell and F. Tramontano, "Next-to-leading order corrections to W t production and decay", *Nucl. Phys.* **B726** (2005) 109–130, arXiv:hep-ph/0506289. doi:10.1016/j.nuclphysb.2005.08.015.

[25] J. M. Campbell, R. K. Ellis, and F. Tramontano, "Single top production and decay at next-to-leading order", *Phys. Rev.* **D70** (2004) 094012, arXiv:hep-ph/0408158. doi:10.1103/PhysRevD.70.094012.

[26] CMS Collaboration, "Performance of Muon Identification in pp Collisions at $\sqrt{s} = 7$ TeV", *CMS Physics Analysis Summary* **CMS-PAS-MUO-10-002** (2010).

[27] CMS Collaboration, "Electron Reconstruction and Identification at $\sqrt{s} = 7$ TeV", *CMS Physics Analysis Summary* **CMS-PAS-EGM-10-004** (2010).

[28] M. Cacciari, G. P. Salam, and G. Soyez, "The Anti-k(t) jet clustering algorithm", *JHEP* **0804** (2008) 063, arXiv:0802.1189. doi:10.1088/1126-6708/2008/04/063.

[29] CMS Collaboration, "Commissioning of the Particle-Flow reconstruction in Minimum-Bias and Jet Events from pp Collisions at 7 TeV", *CMS Physics Analysis Summary* **CMS-PAS-PFT-10-002** (2010).

[30] CMS Collaboration, "Determination of the Jet Energy Scale in CMS with pp Collisions at $\sqrt{s} = 7$ TeV", *CMS Physics Analysis Summary* **CMS-PAS-JME-10-010**.

[31] CMS Collaboration, "CMS MET Performance in Events Containing Electroweak Bosons from pp Collisions at $\sqrt{s} = 7$ TeV", *CMS Physics Analysis Summary* **CMS-PAS-JME-10-005** (2010).

[32] CMS Collaboration, "Algorithms for b Jet identification in CMS ", *CMS Physics Analysis Summary* **CMS-PAS-BTV-09-001** (2009).

[33] D0 Collaboration, "Measurement of the t anti-t production cross section in p anti-p collisions at s**(1/2) = 1.96-TeV using secondary vertex b tagging", *Phys. Rev.* **D74** (2006) 112004, arXiv:hep-ex/0611002. doi:10.1103/PhysRevD.74.112004.

[34] CMS Collaboration, "Performance of muon identification in pp collisions at $\sqrt{s} = 7$ TeV", *CMS Physics Analysis Summary* **CMS-PAS-MUO-10-002** (2010).